

Article

Fast Arc Detection Technology Based on Fractal Dimension for SADA Slip Ring in Satellite Power System

Yanchen Meng ^{1,2} , Enchao Zhang ^{1,2}, Donglai Zhang ^{1,2,*} , Xueli Zhu ^{1,2}, Hongyu Zhu ³ and Anshou Li ²

¹ College of Mechanical Engineering and Automation, Harbin Institute of Technology (Shenzhen), Shenzhen 518055, China; mengyanchen@stu.hit.edu.cn (Y.M.); zhangenchao2021@hit.edu.cn (E.Z.); zhuxueli@stu.hit.edu.cn (X.Z.)

² Peng Cheng Laboratory, Shenzhen 518000, China; anshouli@aliyun.com

³ Shenzhen Aerospace New Power Technology Company, Ltd., Shenzhen 518055, China; zhuhongyu@casc-htxy.com

* Correspondence: zhangdonglai@hit.edu.cn; Tel.: +86-0755-26033998

Abstract: The solar array drive assembly (SADA) slip ring is a critical link that provides electrical power and electric signal transmission between solar arrays and satellite power systems, which is prone to arc faults in the space environment. If these arc faults cannot be detected and eliminated quickly enough, they will seriously threaten the safety of the satellite power system and the satellite. In this paper, a fast arc detection method based on fractal dimension is proposed that adapts to different operating modes of power systems. The detection method collects the current differential signal data flowing through the SADA slip ring, and, according to the trend of the fractal dimension change in this signal, the fault identification algorithm is designed for different operating modes of the power system to achieve real-time and rapid identification of arc faults. Finally, the effectiveness of the proposed method is demonstrated using test data under several different fault conditions.

Keywords: arc fault; fractal dimension; solar array drive assembly; sequential switching shunt regulator (S3R); satellite



Citation: Meng, Y.; Zhang, E.; Zhang, D.; Zhu, X.; Zhu, H.; Li, A. Fast Arc Detection Technology Based on Fractal Dimension for SADA Slip Ring in Satellite Power System. *Energies* **2024**, *17*, 1093. <https://doi.org/10.3390/en17051093>

Academic Editors: Joao L. Afonso and Vitor Monteiro

Received: 24 January 2024

Revised: 18 February 2024

Accepted: 20 February 2024

Published: 25 February 2024



Copyright: © 2024 by the authors. Licensee MDPI, Basel, Switzerland. This article is an open access article distributed under the terms and conditions of the Creative Commons Attribution (CC BY) license (<https://creativecommons.org/licenses/by/4.0/>).

1. Introduction

The solar array drive assembly (SADA) is an important component of a long-life high-power satellite electrical transmission link, which completes the electrical power and electrical signal transmission between the solar panels and the satellite through the internal slip ring [1]. SADA is installed at the junction of the satellite body and the external space environment, which is directly exposed to the space plasma environment and is susceptible to arc faults caused by the charging and discharging effects [2]. The arc fault can lead to fatal failure of the SADA, resulting in loss of power to satellites, thus, threatening the operating life of the satellites in orbit [3].

The structure of disc slip ring is shown in Figure 1; the brushes maintain sliding contact with the slip rings on the disc, which inevitably produces metal wear debris. This debris subsequently accumulates between the internal solder joint of the slip ring and/or between the ring and the solder joint, forming a short-circuit channel and increasing the risk of a vacuum arc discharge [4,5]. The SADA arc fault was initially reported by NASA [6]. To this day, SADA remains one of the main higher-risk components of a satellite [7]. When researching and developing high-voltage bus systems for satellites, assessing the risk of electrical breakdown for SADA slip rings is crucial [8]. In recent years, mechanism analysis and ground equivalent experiments have confirmed the risk of space arc faults in SADA slip rings [8–10]. The power system experiences faults such as reduced solar array power supply capacity, frequent changes in the SR operation modes, reduced bus voltage quality, and even ablation of the solar wings [11], depending on the working conditions and locations of the arc faults. Arc faults can be highly destructive and spread quickly, making them

difficult to contain. They can also spread to adjacent slip rings, causing the power supply and distribution subsystem to fail to output power.

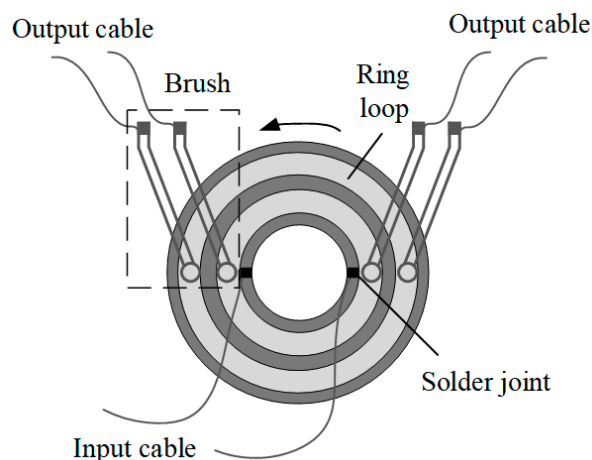


Figure 1. Disc slip ring structure diagram [4].

However, the hidden dangers of arc faults of SADA are not being taken seriously in the current satellite power system design development process, and there are still no corresponding countermeasures to detect and eliminate the arc faults. In other fields such as photovoltaic systems and distribution networks, arc fault detection technology has a certain research foundation, which can be used for reference by SADA arc fault. Reference [12] summarized the series arc fault (SAF) detection technologies for photovoltaic systems using the following four categories: remote detection techniques [13], time-domain methods, frequency-domain methods, and hybrid techniques. Among these four general techniques, both the time-domain [14] and frequency-domain [15,16] detection methods are based on the current and voltage signals in the circuit, and hybrid detection technology combines the time-domain and frequency-domain signal characteristics [17,18]. The main fault diagnosis methods are spectrum analysis, wavelet analysis, and artificial intelligence [19], and arc fault detection technology has seen improvements in terms of its feature extraction and fault detection algorithms in recent years. For example, a blind-source separation algorithm based on principal component analysis (PCA) was used to extract feature quantities to identify series arc faults in [12]. An arc detection neural network based on temporal convolution network is used to extract current waveform features in [20]. An adaptive local mean decomposition algorithm is used to decompose the current samples into production functions representing information from different frequency bands to characterize the arc fault in [21]. The arc faults are detected through zero-range density analysis using the difference in fluctuation characteristics to prevent false detection in [22]. In [23], the dual-tree complex wavelet transform and kernel extreme learning machine are used to decompose the current signal accurately and fuse the characteristic information required for SAF detection; fast and accurate SAF detection was achieved and the system dynamic transient showed good reliability and stability at the same time. The fractal dimension characteristics of the current and voltage signals are also the valid eigenvalues for arc identification [24–26]. Some researchers also used a combination of machine learning and artificial intelligence algorithms [27,28]. For example, a fault detection algorithm based on multiresolution signal decomposition was used for feature extraction in [29], and a two-stage support vector machine (SVM) classifier was used to perform decision making. The use of these methods improves the intelligence level and enhances the fault detection accuracy.

There are two main satellite power system architectures for space applications, the maximum power point tracking (MPPT) architecture and the sequential switching shunt regulator (S3R) architecture. The former is mainly used in small-power satellites, and its power supply principle is similar to that of a terrestrial photovoltaic power system [30,31],

and the satellite power supply systems of such architectures can be borrowed from the existing terrestrial arc detection technology. While the latter is mainly used in medium- and high-power satellites, whose system structure is more complex, arc faults are more hazardous, and there is no applicable arc detection method. High-voltage high-power power systems usually has a sufficient number of shunt regulators, and the voltage and current levels of individual shunt branches are very high, resulting in an arc fault that can easily spread out of control. Therefore, the high-voltage high-power satellite platform needs to focus on detection speed and practicality in the arc start “spark” stage to effectively identify and cut off the source of hidden problems, blocking the spread of the fault. Remote detection is sensitive to space interference factors, and complex algorithms such as artificial intelligence algorithms are problematic in that they require large numbers of calculations and additional computing equipment, and the calculation process is unpredictable and uninterruptible [12], making these methods difficult to implement in space environments.

A SADA arc fault is not easy to predict and control, and the complexity of the satellite power supply operation mode increases the difficulty of its detection and protection, resulting in this problem not yet being solved. To address the abovementioned issues, a fast detection method for SADA arc faults is proposed in this paper that is based on the fractal dimension. According to the trend of fractal dimension in different operating modes of the power system, the arc identification algorithm is designed to detect arc faults in real time. The method is relatively simple, fast, and easy to realize and apply in space environment.

The contribution of this paper is summarized as follows: we design a fast arc fault detection method according to the characteristics of SADA arc faults and different operating modes of shunt regulators (SR). The method is based on the fractal dimension characteristics of the arc current signal, and realizes real-time and fast arc fault detection through efficient arc recognition algorithms. The method can recognize the arc faults of SADA slip ring and eliminate the faults in time before they spread, which effectively ensures the safety of the satellite power system.

This paper is organized as follows: In Section 2, the operating mode and principle of the satellite power system are introduced first. Then the fractal dimension characteristics of the arc faults are analyzed in Section 3, and, on this basis, the fast arc fault detection method and fault identification algorithm for the SADA slip ring are designed in Section 4 according to the fractal dimension characteristics of three operating modes. In Section 5, the effectiveness of the proposed method is demonstrated using test data under several different fault conditions. Finally, Section 6 draws a conclusion from the paper.

2. Satellite Power System

High-power satellite power systems usually use a power controller based on the sequential switching shunt regulator (S3R) architecture. Figure 2 shows a schematic diagram of the S3R architecture. The solar arrays are divided into identical sections, which are then connected to corresponding shunt regulators (SRs) through the SADA slip rings to form one-to-one solar array to SADA slip ring to SR correspondences. The output terminals of all shunt regulators are connected in parallel to the bus (V_{bus}) to convert the constant current output of the solar array into a constant bus voltage.

A typical shunt regulator (SR) topology is illustrated in Figure 3 [32], where R_R is the contact resistance of SADA slip ring and L_H is the harness inductance. The I_{max} control driver and L_1 suppress the current stress of the shunt Mosfet Q_1 . There are three operating modes of each SR. In bus feeding mode, the SR delivers all the power from the solar array to the bus, and the SA operates at the rated working point (point 2), as shown in Figure 4a. In shunt mode, the SR shunts all the power from the solar array to ground, and the SA operates at the short circuit working point (point 1), as shown in Figure 4b. In switching mode, the SR switches between the bus feeding mode and shunt mode, thus modulating the power delivered to the bus, and the working point of SA switches between the two points correspondingly.

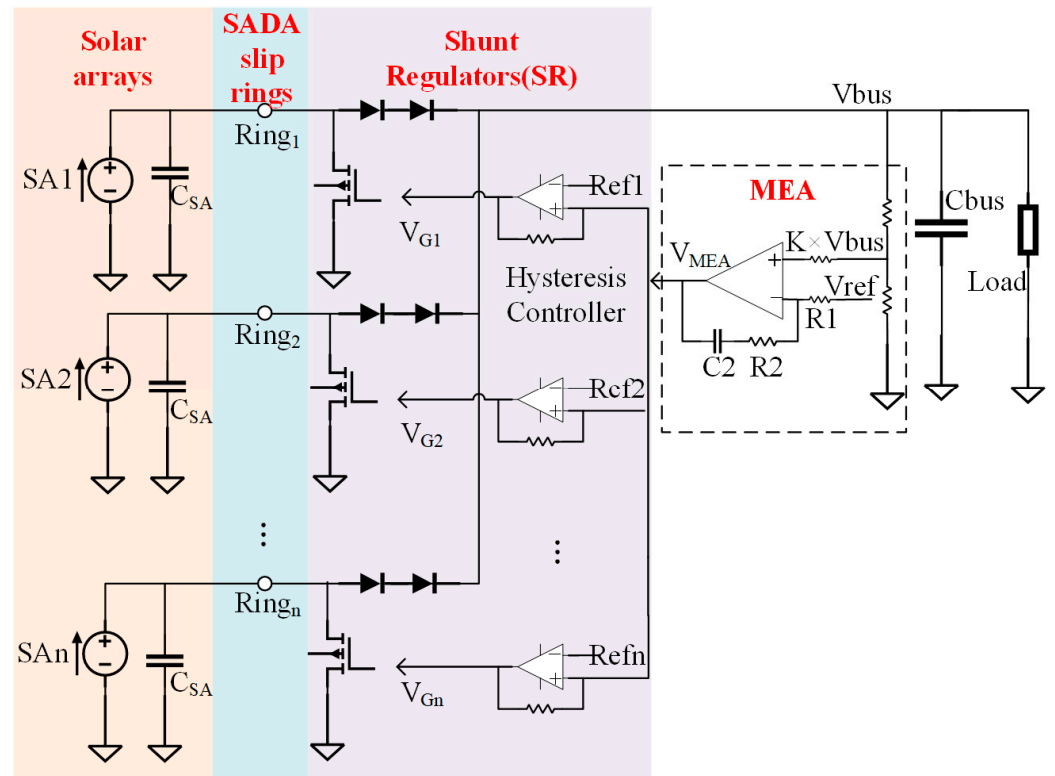


Figure 2. Schematic diagram of S3R.

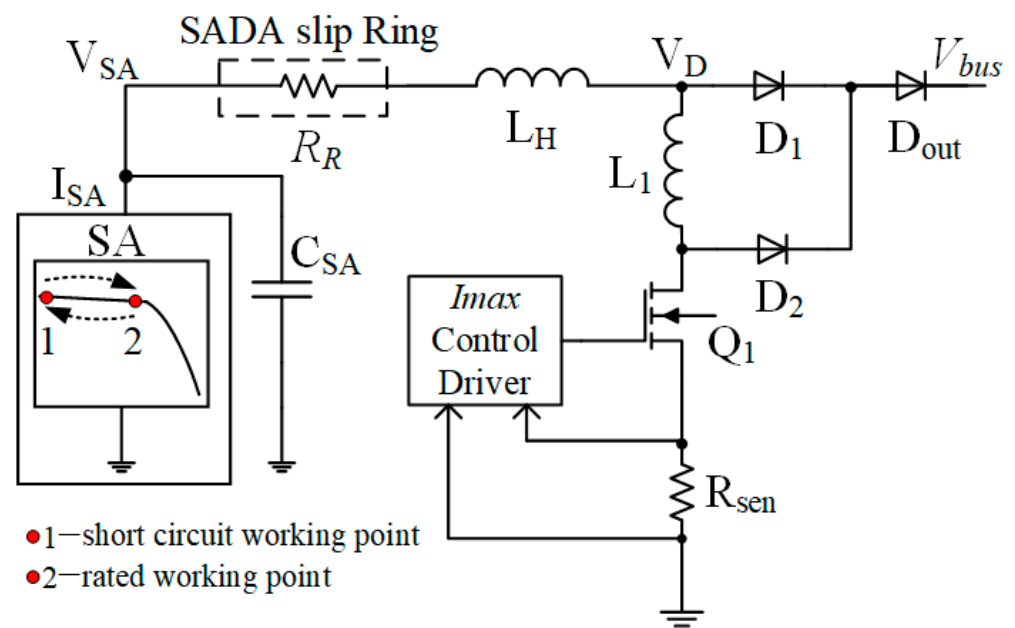


Figure 3. Shunt regulator (SR) topology.

The operating mode of each section’s SR is determined by the mean value of the payload power demand [33]. In steady-state conditions, it is generally ensured that only one shunt regulator operates in switching mode while the others remain in bus feeding mode or shunt mode.

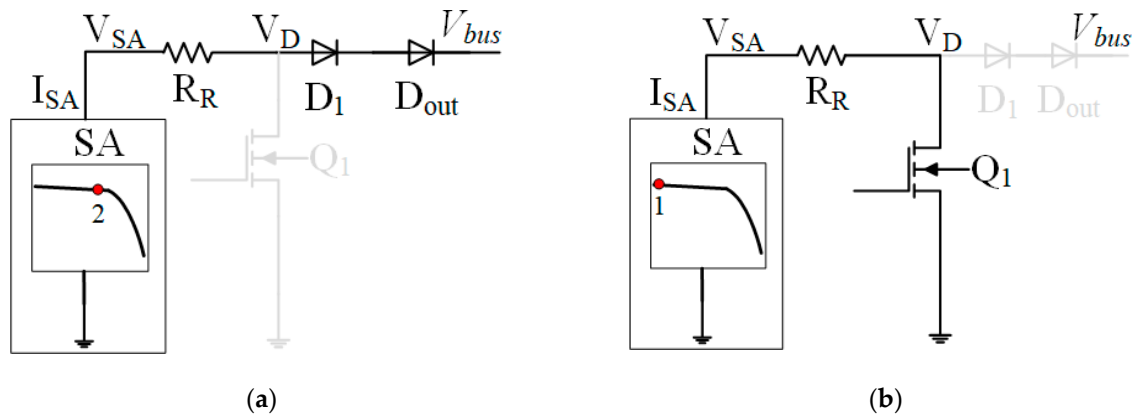


Figure 4. Schematic diagram of SR operation mode. (a) Bus feeding mode. (b) Shunt mode.

3. Arc Characteristic Analysis

3.1. Fractal Dimensional

Fractal geometry is a branch of mathematics that describes the complex forms of nature. Fractal dimension is used in fractal theory to describe different fractal features. In the engineering field, fractal dimension is widely used in signal processing as a measure of signal complexity. The regularity of the arc fault signal and the steady-state operation signal of the system current is different. In the steady-state operation stage, a relatively stable fractal dimension value is shown; in the process of the stable operation stage turning to the arc fault stage, the fractal dimension value will appear with a large difference and with a good regularity, so the trend of the fractal dimension value can be used as a basis for arc fault identification. The fractal dimension of the signal in the two-dimensional plane is calculated as follows:

Assume that the signal to be fractalized is a curve X in the two-dimensional plane, and if the length of X is measured by straight-line segments of length l , $N(l)$ segments are required. For different lengths of l , there exists a constant value C , which makes Equation (1) valid, where the finite real number D is the fractal dimension of the signal X to be fractalized.

$$\lim_{l \rightarrow 0} N(l) \cdot l^D = C, \quad (1)$$

Among them, $N(l)$, D , and C are unknown, and the number of $N(l)$ is huge when l tends to 0. Therefore, this idea is only a theoretical derivation and can be used for mathematical analysis, but it is difficult to realize numerical calculation.

In practical applications, the common methods for measuring fractal dimension include associative dimension, generalized dimension, and box dimension, among which the box dimension method is widely used because of its high computational accuracy and low computational effort.

Calculating the fractal dimension by the box dimension method is equivalent to placing the signal to be fractalized in a uniformly partitioned grid and finding the minimum number of cells needed to cover this fractal. The idea is to take a box with side length ε . Assume that the continuous time series signal $x(t) \in F$, and F is some bounded subset of R^n , and use this box to cover the signal to be fractalized, then count the number of non-empty boxes containing the signal curve, which is counted as $N(\varepsilon)$. The side lengths of the box are reduced in turn and the corresponding $N(\varepsilon)$ is calculated until ε tends to 0. By calculating a series of ε and $N(\varepsilon)$, the linear relationship is fitted by least squares in double logarithmic coordinates, and the slope of the resulting line is the fractal dimension D of the signal to be measured, as in Equation (2).

$$D = \lim_{\varepsilon \rightarrow 0} (\log_2 N(\varepsilon)) / (-\log_2(\varepsilon)) \quad (2)$$

3.2. Arc Testing and Fractal Dimensional Characterization

When the power system is in steady-state operation, SADA series arc faults in single sections of SR can be equated to a DC series arc fault for arc characterization. The series current differential signal V_{CT} data are collected to verify the correlation between the arc fault signal and the fractal dimension. V_{CT} is converted by a current transformer (CT). Waveforms are monitored by a waveform memory recorder with a sampling frequency of 1 MHz. The arc generator as shown in Figure 5 is connected in series to the DC voltage source loop to simulate the arc fault (SAF).

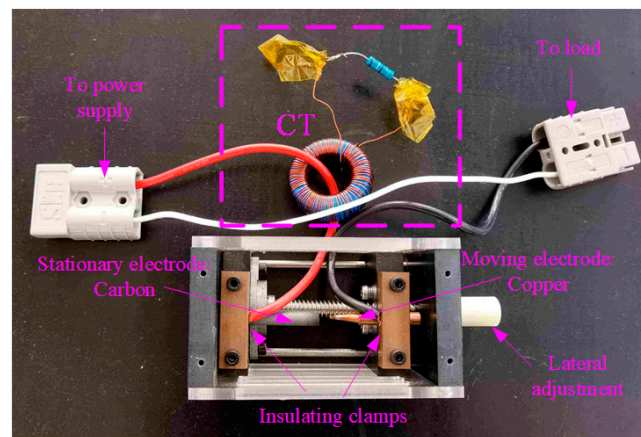


Figure 5. Arc generator.

The trend of the fractal dimension is calculated by extracting the data segment for a total of 0.1 s before and after the moment of arc fault occurrence, and comparing it with the original current differential signal at the same moment one-by-one, as shown in Figure 6 (45 V, 2.25 A, resistor load).

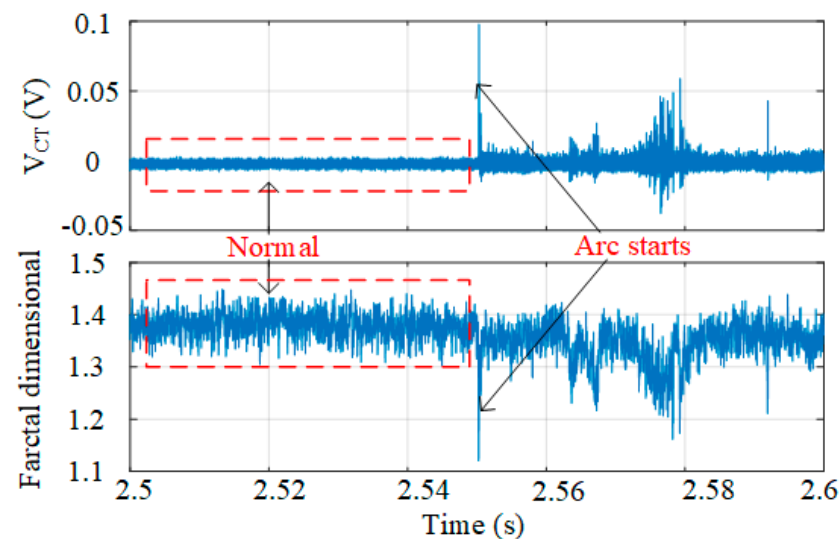


Figure 6. Variation trend of fractal dimension of current differential signal before and after arc fault.

It can be seen that the signal regularity of V_{CT} in the arc fault stage and steady-state operation stage is different. During the steady-state operation of the system, the fractal dimension of the measured current differential signal is distributed in a stable interval, while when an arc fault occurs, the fractal dimension value appears to vary significantly with the change in V_{CT} amplitude and frequency, and decreases sharply at the moment of arc fault occurrence accordingly, which is clearly distinguished from the steady-state

value. Therefore, the trend of the fractal dimension value can be used as the basis of arc fault identification.

4. Arc Fault Detection Method

On the basis of the above fractal dimensional characteristics of the arc, the SADA fast arc fault detection scheme was designed, as shown in Figure 7. The arc detection system includes the satellite power system to be tested, signal sampling and conditioning link, data processing link, arc identification link, and arc extinguishing link. Among them, the satellite power system to be tested includes solar array, SADA slip ring, shunt regulator, etc. The differential current signal V_{CT} of the SADA slip ring is collected to detect the arc fault.

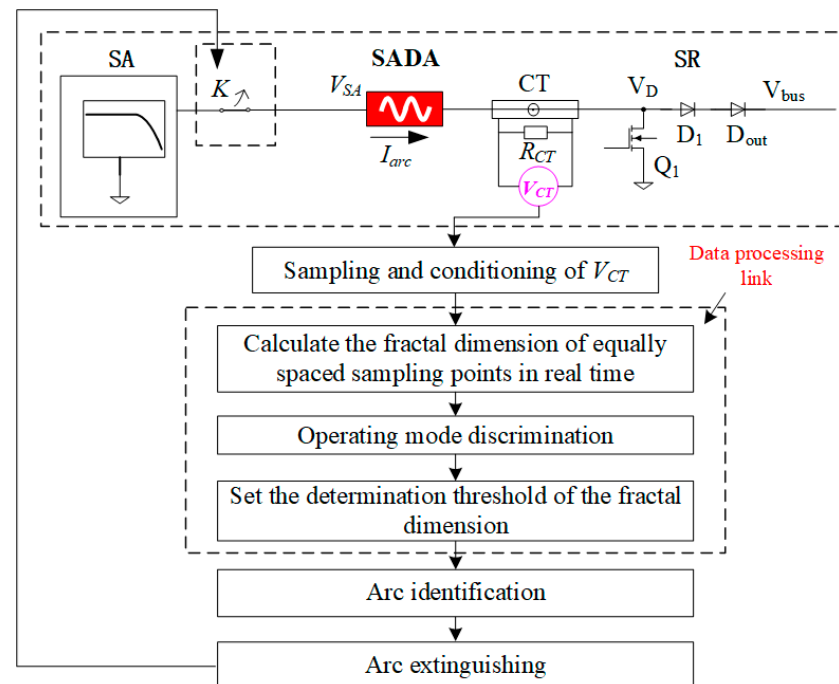


Figure 7. SADA arc fault detection system.

The workflow of arc fault detection is described as follows:

- (1) Signal sampling and conditioning link to collect the current differential signal V_{CT} ;
- (2) In the data processing link, the fractal dimension value of the current differential signal at equally spaced sampling points is calculated in real time, and the operating mode of the corresponding shunt regulator is determined based on the fractal dimension value in steady-state operation, and the threshold values for arc identification in different operating modes are set;
- (3) Arc identification link runs through the arc fault identification algorithm to determine whether an arc fault occurred in power system to be tested;
- (4) If the SADA slip ring is judged to have an arc fault, the system will be interrupted by the arc extinguishing link, and the switch K will be disconnected to quickly cut off the arc to prevent the fault from spreading and to avoid further damage to the system caused by the arc fault to ensure safe and reliable operation of the system.

4.1. Fractal Dimensional Characteristics Analysis of Three Operating Modes

Take 100 sampling points as a group to read the current differential data V_{CT} in real time, and recurse one sampling point successively to obtain the following array: $[V_{1,1}, V_{1,2} \dots V_{1,99}, V_{1,100}]$, $[V_{2,1}, V_{2,2} \dots V_{2,99}, V_{2,100}] \dots [V_{n,1}, V_{n,2} \dots V_{n,99}, V_{n,100}]$, then calculate the fractal dimension values of each array in real time: $[D_1, D_2 \dots D_n]$.

According to the above calculation rules, the typical variation trend of the fractal dimension of V_{CT} before and after the arc fault in the three operating modes is shown

in Figure 8. The fractal dimension values of bus feeding mode are shown in Figure 8a. During normal operation, the fractal dimension is steadily distributed around 1.4, and the moment the arc fault occurs, it drops sharply to below 1.3, and continues to fluctuate unsteadily afterwards.

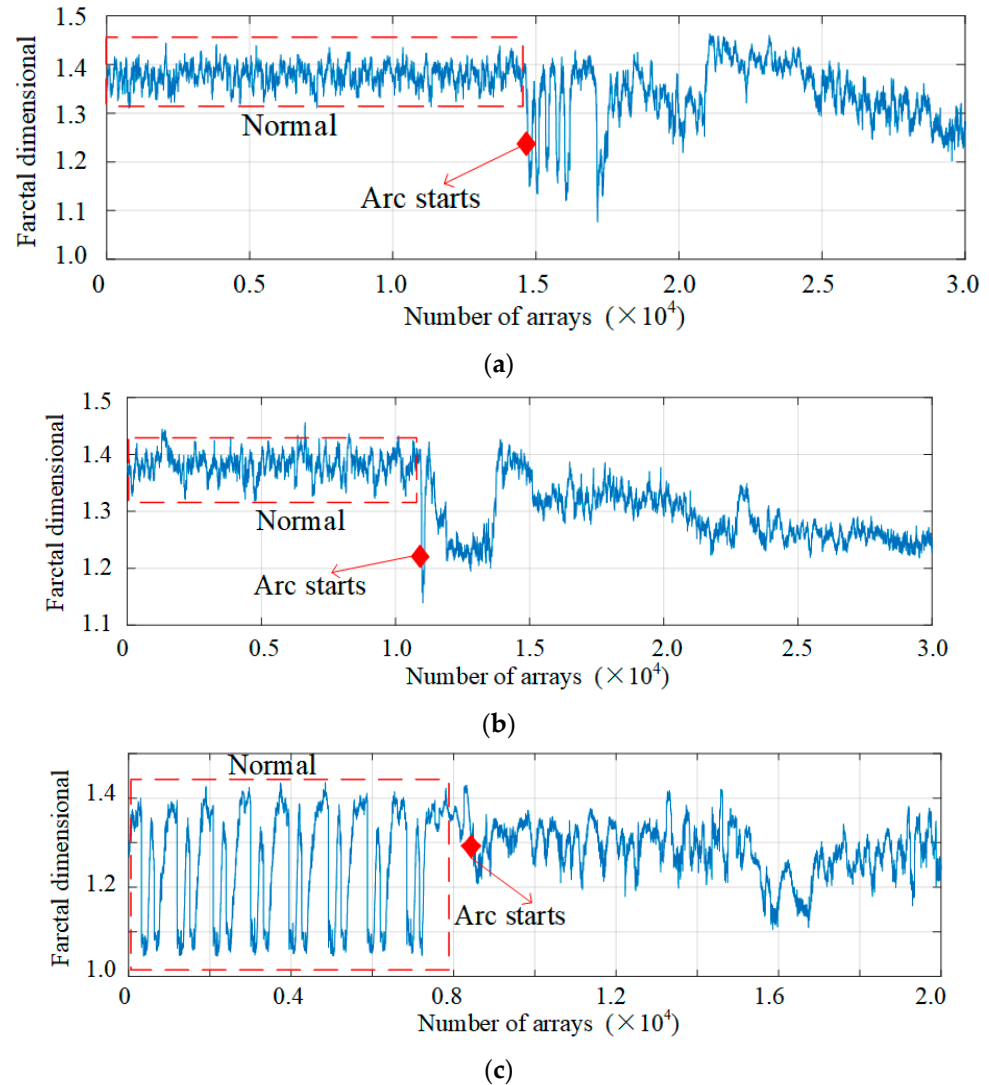


Figure 8. Variation trend of fractal dimension of VCT before and after arc fault. (a) Bus feeding mode. (b) Shunt mode. (c) Switching mode.

The fractal dimension values of shunt mode are shown in Figure 8b. As with the bus feeding mode, the current is a stable DC signal during steady-state operation, so the trend of the fractal dimension is the same as that of the bus feeding mode.

The fractal dimension values of switching mode are shown in Figure 8c. During the steady-state operation, the fractal dimension changes periodically and regularly. When an arc fault occurs, the periodic change is interrupted and the dimension is concentrated between 1.2 and 1.3.

4.2. Arc Identification

The flow of the SADA arc fault detection procedure based on fractal dimension and arc identification algorithm is shown in Figure 9. During system operation, the V_{CT} data are always read in real time in groups of 100 sampling points and recursively one point at a time to obtain the arrays: $[V_{1,1}, V_{1,2}, V_{1,99}, V_{1,100}]$, $[V_{2,1}, V_{2,2}, \dots, V_{2,99}, V_{2,100}]$, ... $[V_{n,1}, V_{n,2}, \dots, V_{n,99}, V_{n,100}]$. The fractal dimension values for each array are calculated

in real time: $[D_1, D_2 \dots D_n]$. The arc fault detection procedure process is divided into two stages: operating mode discrimination and fault identification. The specific process is as follows:

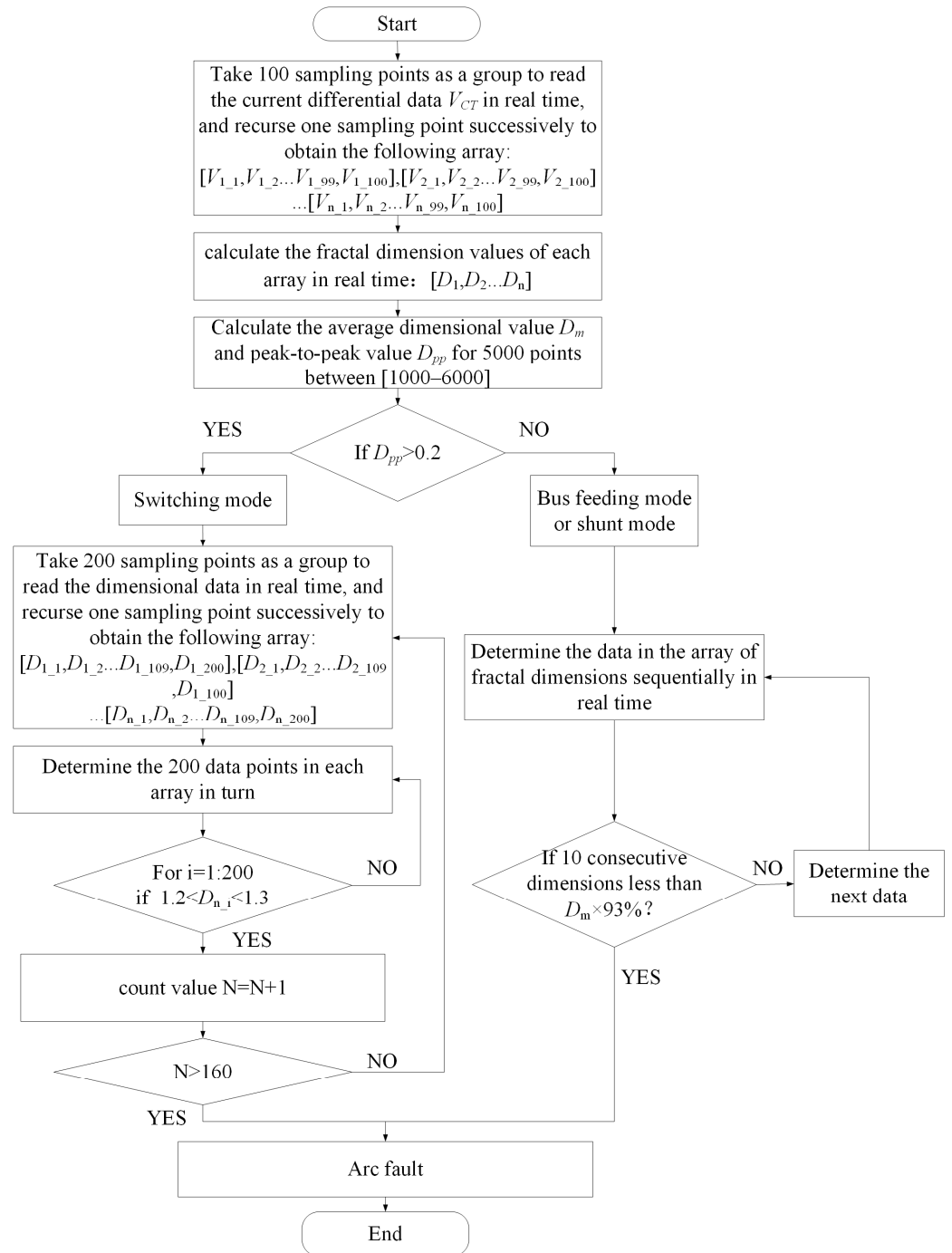


Figure 9. Flow chart of arc fault identification.

(1) Operating mode discrimination

During steady-state operation, calculate the average dimensional value D_m and the peak-to-peak value D_{pp} for 5000 points between (1000–6000). From the analysis above, it is clear that the bus feeding mode and shunt mode have the same trend of fractal dimensional change, so only D_{pp} is needed to distinguish the switching mode from the two: if D_{pp} is greater than 0.2, it is the switching mode, otherwise it is the bus feeding mode or shunt mode.

(2) Arc fault identification

It can be seen from Figure 8 that the fractal dimension distribution interval is stable during the steady-state operation of bus-powered mode and shunt mode, while it drops sharply at the time of arc fault. Based on this characteristic, a fault determination threshold can be set by a threshold factor based on the average value of the fractal dimension D_m during steady-state operation. The fractal dimension varies periodically during the steady-state operation of the switching mode, but the dense distribution interval (1.2~1.3) of the dimension at the beginning of the arc can be clearly distinguished from the high dimension interval (1.3~1.4) and the low dimension interval (1.1~1.2) during the steady-state operation, so the arc fault identification can still be performed according to the distribution characteristics.

Based on the above feature analysis, the arc fault identification algorithm is designed.

If the operating mode is bus feeding mode or shunt mode: Set the threshold to the average D_m of 5000 dimensional values during steady-state operation multiplied by 93%. When 10 consecutive values in the dimension array are less than the threshold, an arc fault is determined to have occurred.

If the operating mode is switching mode: Take 200 sampling points as a group to read the dimensional data in real time, and recurse one sampling point successively to obtain the following array: $[D_{1_1}, D_{1_2}, \dots, D_{1_{109}}, D_{1_{200}}], [D_{2_1}, D_{2_2}, \dots, D_{2_{109}}, D_{2_{200}}], \dots, [D_{n_1}, D_{n_2}, \dots, D_{n_{109}}, D_{n_{200}}]$. Determine the 200 data points in each array in turn, and if the number of points distributed between 1.2~1.3 is greater than 160, it is determined that an arc fault has occurred.

5. Experimental Verification

To further evaluate the performance of the proposed fault detection method in practice, a two-section shunt regulator system was set up for experiments, as shown in Figure 10. Each SR of the system was fed by an Agilent E4360A solar (Santa Clara, CA, USA) array simulator and loaded with an electronic load (ITECH IT8834S) (ITECH, South Burlington, VT, USA). The parameter configuration of the U–I characteristic curve was $V_{OC} = 115$ V (open circuit), $V_{MP} = 105$ V, $I_{MP} = 7$ A (maximum power point), and $I_{SC} = 7.8$ A (short circuit). The arc generator was used to simulate the arc fault of SADA slip ring. The data sampling rate was 1 MHz. The shunt regulator adopts the topology shown in Figure 3, and its various parameters are shown in Table 1.

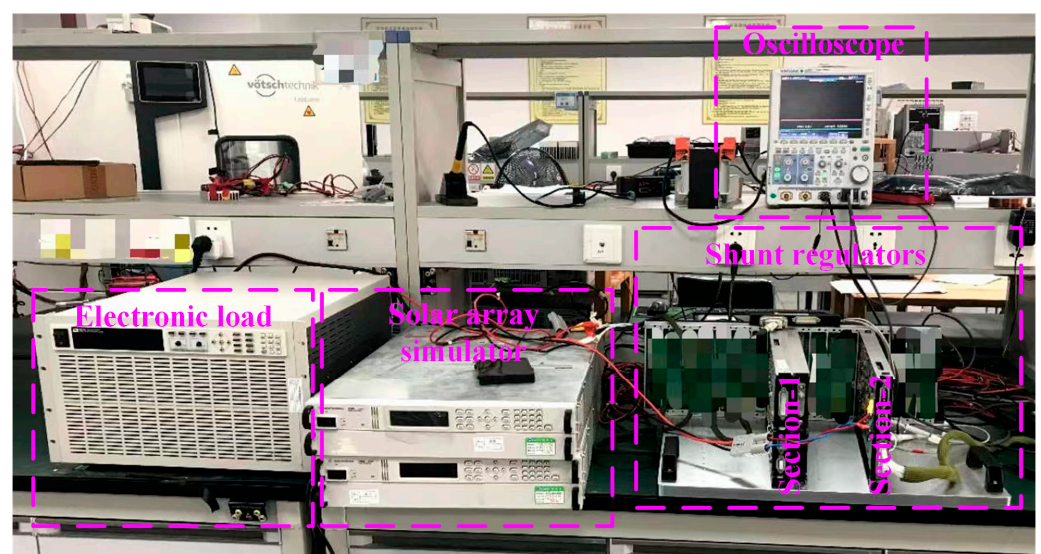


Figure 10. Experimental platform.

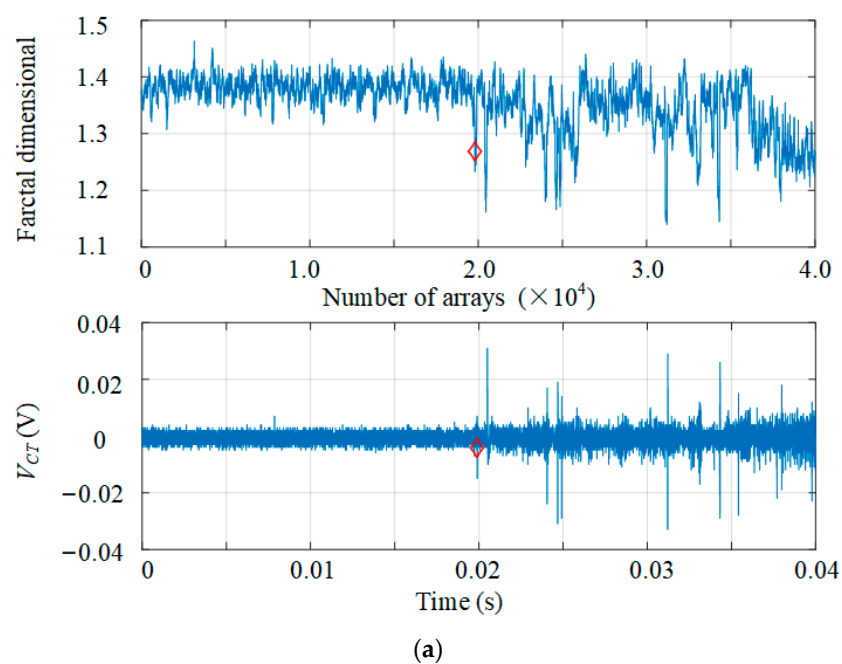
Table 1. Parameters of platform.

Parameter	Value
Bus voltage	100 V
Bus voltage ripple	600 mV
Solar array sections	7 A × 2 sections (can be extended to 7 A × 24 sections)
Harness inductance L_H	28 μ H
Power inductor L_1	60 μ H
The sampling resistor R_{sen}	2.5 m Ω
Bus capacitance	3.0 mF
MEA voltage divider K	0.064
MEA: R_1	2.35 k Ω
MEA: R_2	103.75 k Ω
MEA: C_1	10 nF
Current transformer (CT)	1:100
R_{CT}	6.8 Ω

The two-section system has two conventional operating conditions: (1) SR-2 is in bus feeding mode and SR-1 is in switching mode; (2) SR-2 is in switching mode and SR-1 is in shunt mode. The two working conditions contain the three working modes of SR. Two typical cases are selected in each of three operating modes to verify the fractal dimension-based arc detection. The operating condition settings and their arc detection results are shown in Table 2. Two loads of 6.5 A and 3.5 A are set in shunt mode, and two loads of 10.5 A and 13.5 A are set in bus feeding mode and switching mode, and their typical data analysis processes based on fractal dimension are shown in Figures 11–13, respectively.

Table 2. Arc fault detection conditions and results.

Operating Condition of S3R	Load	Position of Arc	Test Results
SR-1 Shunt mode	0 A		(10/10)
SR-2 Switching mode	6.5 A	SR-1	(10/10)
SR-1 Switching mode	3.5 A	SR-2	(10/10)
SR-2 Switching mode	3.5 A	SR-1	(10/10)
SR-2 Bus feeding mode	13.5 A	SR-2	(10/10)
SR-1 Bus feeding mode	13.5 A	SR-1	(10/10)

**Figure 11.** Cont.

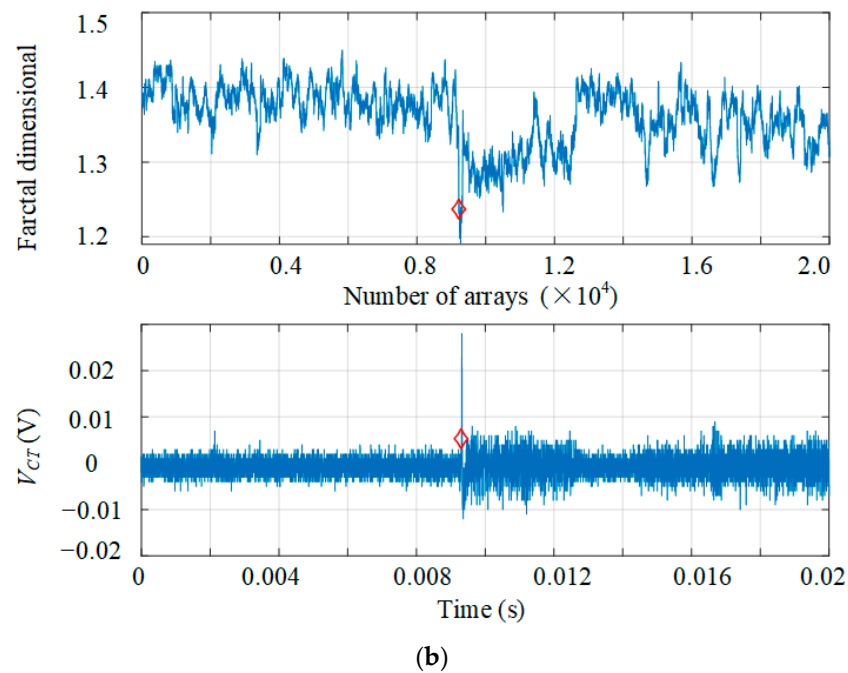


Figure 11. Arc identification results based on fractal dimension of shunt mode: (a) 6.5 A load, (b) 3.5 A load.

The arc fault identification process based on fractal dimension for shunt mode is shown in Figure 11. Under the same load conditions, the figure below is the real-time sampling data of the current differential signal V_{CT} . The figure above shows the real-time fractal dimension, which corresponds to an array of 100 data (100 μ s) recursively forward at each moment of sampling. The red diamond marker points to the arc fault identification moment.

The fractal dimension value distribution is stable during the normal operation of shunt mode, and decreases sharply at the moment of arc fault occurrence. According to the arc identification algorithm, when 10 consecutive real-time fractal dimensions are less than 93% of the average value of the dimension at steady state, it can be determined that an arc fault has occurred.

Comparing the real-time fractal dimension values and V_{CT} sampling data in Figure 11, it is obvious that the fault can be detected in time when the V_{CT} signal fluctuates slightly due to the arc being under different load conditions.

The arc fault identification process based on fractal dimension for bus feeding mode is shown in Figure 12. As with the detection process of shunt mode, the real-time fractal dimension and V_{CT} sampling data have a good correspondence. Therefore, the trend of fractal dimension can be used to detect the arc fault under different load conditions of bus supply mode efficiently in real time. It is obvious from Figure 12 that the arc fault of different energy levels corresponding to the two load conditions can be detected in real time.

The arc fault identification process based on fractal dimension for switching mode is shown in Figure 13. The dimensionality of the switching mode varies periodically during the steady-state operation, and the periodic change is interrupted and the dimension is concentrated between the maximum and minimum values of the steady-state operating period when an arc fault occurs.

The two typical arc fault cases of the switching mode are shown in Figure 13a,b. The former is a case of stable arcing, when an arcing fault occurs, the corresponding solar array power supply capacity decreases, causing the switching mode to switch to bus feeding mode to meet the system power demand. The latter is the case of transient electric spark, when a “small” arc fault affects the power supply quality, but does not change the operating

mode. It is obvious from Figure 13 that both cases can be detected in real time when the arc causes slight fluctuations in the V_{CT} signal, which proves that the arc identification algorithm of the switching mode is sensitive and reliable.

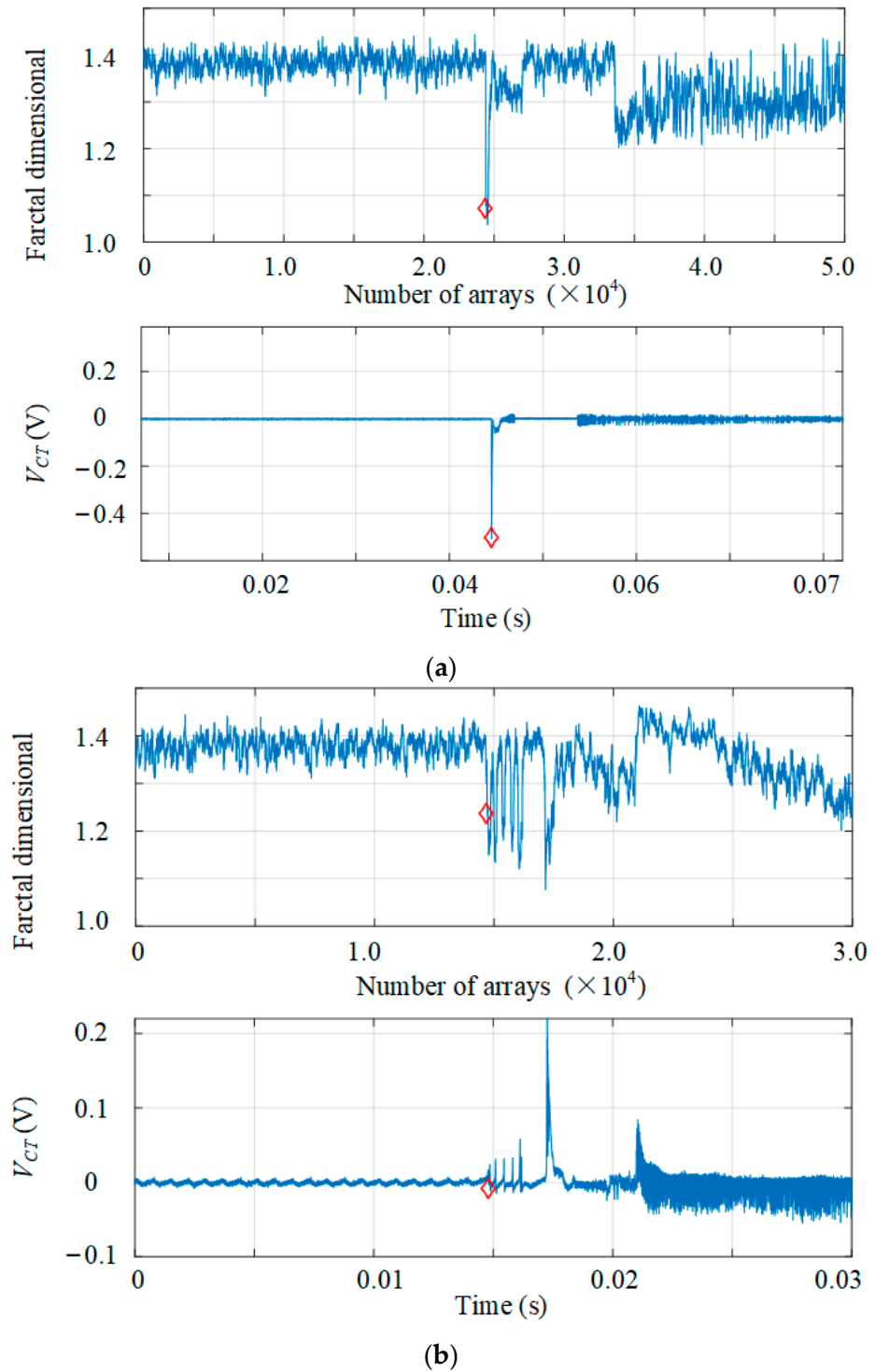


Figure 12. Arc identification results based on fractal dimension of bus feeding mode: (a) 13.5 A load, (b) 10.5 A load.

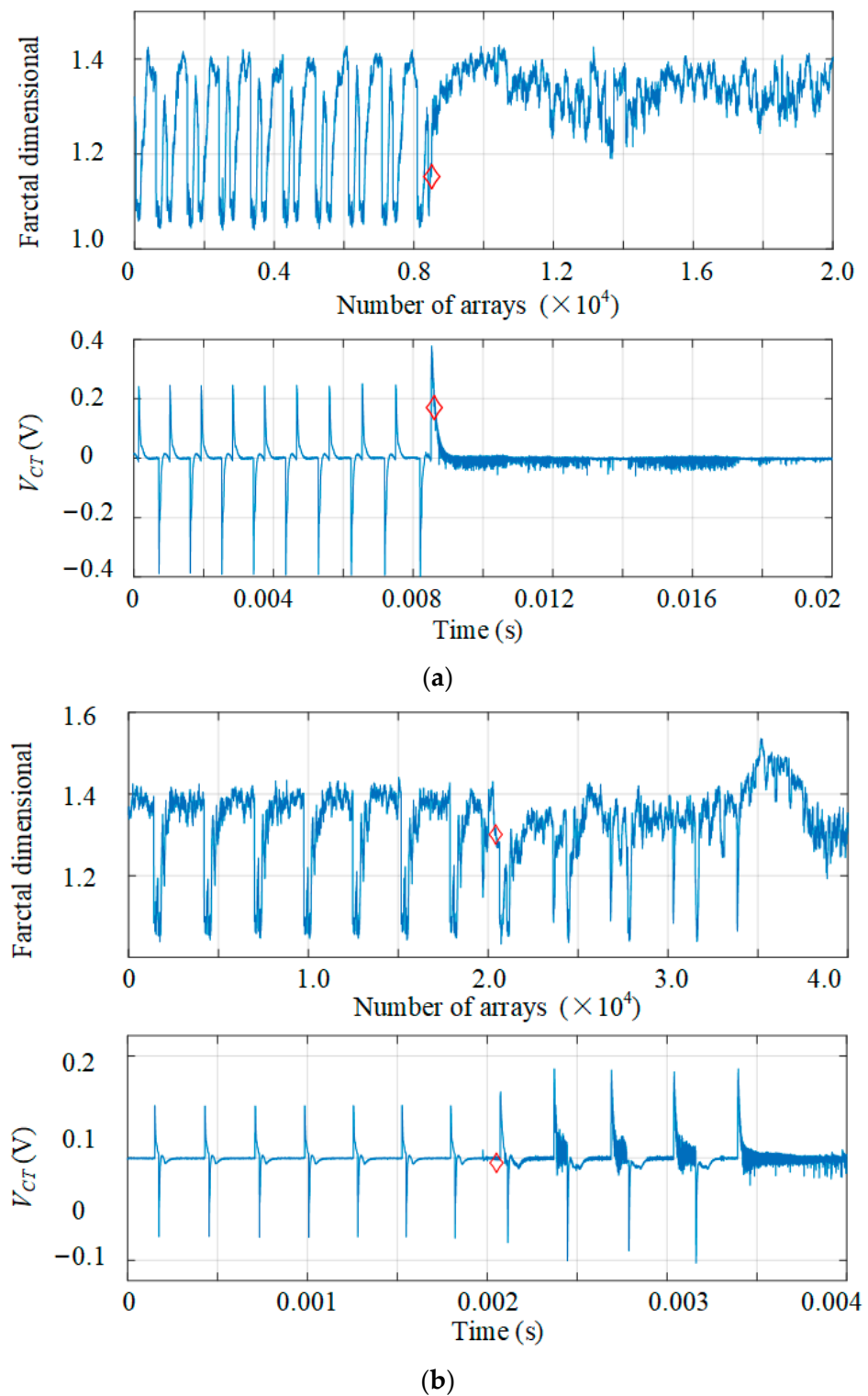


Figure 13. Arc identification results based on fractal dimension of switching mode: (a) 13.5 A load, (b) 10.5 A load.

As shown in Table 2, 10 groups of arc fault simulation experiments were conducted under two typical operating conditions in each operating mode, and the arc faults can be detected in real time by the fractal-dimension-based arc identification algorithm.

The above experimental verification proves that the arc detection method based on fractal dimension can identify the arc fault in real time and quickly when the arc starts,

avoiding the formation of a stable arc and then endangering the safety of the power system and even the satellite.

6. Conclusions

In this paper, a fast arc detection method based on the fractal dimension is proposed for the SADA arc detection of high-voltage high-power satellite power systems. High-voltage high-power power systems usually have a sufficient number of shunt regulators, and the voltage and current levels of individual shunt branches are very high, resulting in an arc fault that can easily spread out of control. The arc fault identification algorithm is designed according to the fractal dimension distribution characteristics of the three operating modes of the power system, which can effectively identify and cut off the source of the hidden problem and stop the spread of the fault when the arc starts. The effectiveness and real-time performance of the fractal-dimension-based detection scheme is demonstrated by multi-group experiments under various working conditions of the three operating modes of the power system.

The shunt regulators have three operation modes and switch between them as the input and output conditions of the power system change. The voltage and current levels, variation intervals, and trends of the system are different in different operating modes, and the potential internal and external disturbances are also different. The switching of the three operating modes will also cause interference to the arc fault detection, so it is necessary to categorize and design the arc recognition algorithm according to the characteristics of each operating mode. Experimental results show that the real-time fractal dimension and V_{CT} sampling data have a good correspondence.

- In the shunt mode and bus feeding mode of the satellite power system, the fractal dimension value distribution is stable during the steady-state operation, and decreases sharply at the moment of arc fault occurrence. The arc fault can be detected in time by arc recognition algorithms when the V_{CT} signal fluctuates slightly due to the arc being under different load conditions;
- In switching mode, the fractal dimension varies periodically during the steady-state operation. The periodic change trend is interrupted when an arc fault occurs and the dimension is concentrated between the maximum and minimum values of the steady-state operating period. Even “small” arc faults can be detected in real time by arc recognition algorithms.

SADA slip rings do not allow arc faults to occur during the mission period in principle, and according to the satellite mission requirements, it is required to effectively detect the arc fault before the fault spreads, i.e., within the millisecond time scale. Therefore, compared with the ground-based detection applications of existing methods, this paper improves the speed of the detection method by designing an efficient arc recognition algorithm.

This arc detection method based on fractal dimension is suitable for high-voltage and high-power satellite power platforms due to its real-time and fast advantages. This power system usually has a large number of shunt regulator arrays, and the voltage and current level of a single array is very high, which leads to an arc fault that can very easily spread out of control. For this kind of power platform, it is required to effectively identify and cut off the source of hidden danger and block the spread of faults at the stage of the “spark” at the beginning of the arc fault.

However, this method also has limitations, because it focuses on the detection speed, resulting in the anti-interference not being strong enough to cause misjudgment. For high-voltage and high-power power platforms, the structure of multiple shunt regulator arrays can avoid the impact of load power supply due to the misjudgment of a single array, but if it is expanded to be applied to medium and low-power platforms, it is necessary to further improve the algorithms to avoid the misjudgment under the premise of trying to ensure the detection speed.

Author Contributions: Conceptualization, D.Z.; methodology, Y.M., E.Z. and D.Z.; formal analysis, Y.M. and E.Z.; investigation, X.Z.; validation, Y.M. and X.Z.; resources, H.Z.; data curation, X.Z.; software, E.Z.; writing—original draft preparation, Y.M.; writing—review and editing, Y.M., H.Z. and A.L.; supervision, H.Z. and D.Z.; project administration, H.Z. All authors have read and agreed to the published version of the manuscript.

Funding: This research was funded by the National Nature Science Foundation of China, grant number 52277174, and the National Key Research and Development Program of China, grant number 2020YFC2201000.

Data Availability Statement: The data presented in this study are available on request from the corresponding author. The data are not publicly available due to author and the confidentiality requirements of the authors' organizations.

Conflicts of Interest: Author Hongyu Zhu was employed by the company Shenzhen Aerospace New Power Technology Company, Ltd. The remaining authors declare that the research was conducted in the absence of any commercial or financial relationships that could be construed as a potential conflict of interest.

References

1. Gao, Y.; Cao, D.; Wei, J.; Huang, W. Modeling for solar array drive assembly system and compensating for the rotating speed fluctuation. *Aerosp. Sci. Technol.* **2019**, *84*, 131–142.
2. Liang, Y.; Wang, C.; Song, S. Development of the Design and Analysis System for the Solar Array Drive Mechanism. In Proceedings of the 6th International Conference on Intelligent Human-Machine Systems & Cybernetics, Hangzhou, China, 26–27 August 2014.
3. Feng, W.; Han, J.; Liu, Y.; Wang, Z.; Xu, Y.; Yu, D. Spacecraft EPDS Arc Short Circuit Failure and Prevention. *Spacecr. Eng.* **2013**, *22*, 65–70.
4. Shen, L.; Wang, X.; Wang, Y.; Jing, G.; Li, C. Vacuum Arc Discharge Test of Aerospace Disc Slip Ring with Metallic Wear Debris. *Spacecr. Environ. Eng.* **2019**, *36*, 463–467.
5. Sun, Y.; Wang, Y.; Sun, X.; Liu, X.; Yu, J. Research on failure modeling and process optimization of transmission conductive slip ring for aerospace. *J. Mech. Eng.* **2020**, *56*, 1–12.
6. Lundin, B.T. *Report of the Seasat Failure Review Board*; NASA Technical Reports Server (NTRS): Washington, DC, USA, 1978; pp. 1–98.
7. Ji, X.-Y.; Li, Y.-Z.; Liu, G.-Q.; Wang, J.; Xiang, S.-H.; Yang, X.-N.; Bi, Y.-Q. A brief review of ground and flight failures of Chinese spacecraft. *Prog. Aerosp. Sci.* **2019**, *107*, 19–29. [[CrossRef](#)]
8. Avino, F.; Gaffinet, B.; Bommottet, D.; Howling, A.; Furno, I. Slip Ring Test Assembly with Increased Breakdown Voltage Limit for High-Voltage Bus Satellites. *IEEE Aerosp. Electron. Syst. Mag.* **2020**, *35*, 32–36. [[CrossRef](#)]
9. Wang, X.; Min, D.; Pan, S.; Zheng, S.; Hou, X.; Wang, L.; Li, S. Coupling Effect of Electron Irradiation and Operating Voltage on the Deep Dielectric Charging Characteristics of Solar Array Drive Assembly. *IEEE Trans. Nucl. Sci.* **2021**, *68*, 1399–1406. [[CrossRef](#)]
10. Jing, G.; Shen, L.; Wang, X.; Wang, Y.; Li, C.; Li, W. Experimental study of vacuum charge and discharge of the slip ring in spacecraft solar array drive mechanism. *Spacecr. Environ. Eng.* **2021**, *38*, 166–170.
11. Meng, Y.; Zhang, D.; Wang, C.; Liu, Z.; Zhu, L.; Li, A. Modeling and Analysis of Non-Linear Phenomena of Satellite Power System in Space Environment and Hazard-Risk Evaluations. *Electronics* **2022**, *11*, 1756. [[CrossRef](#)]
12. Ahmadi, M.; Samet, H.; Ghanbari, T. A New Method for Detecting Series Arc Fault in Photovoltaic Systems Based on the Blind-Source Separation. *IEEE Trans. Ind. Electron.* **2020**, *67*, 5041–5049. [[CrossRef](#)]
13. Ke, Y.; Zhang, W.; Suo, C.; Wang, Y.; Ren, Y. Research on Low-Voltage AC Series Arc-Fault Detection Method Based on Electromagnetic Radiation Characteristics. *Energies* **2022**, *15*, 1829. [[CrossRef](#)]
14. Georgijevic, N.L.; Jankovic, M.V.; Srdic, S.; Radakovic, Z. The Detection of Series Arc Fault in Photovoltaic Systems Based on the Arc Current Entropy. *IEEE Trans. Power Electron.* **2016**, *31*, 5917–5930. [[CrossRef](#)]
15. Gu, J.; Lai, D.; Wang, J.; Huang, J.; Yang, M. Design of a DC Series Arc Fault Detector for Photovoltaic System Protection. *IEEE Trans. Ind. Appl.* **2019**, *55*, 2464–2471. [[CrossRef](#)]
16. Dołęgowski, M.; Szmajda, M. A Novel Algorithm for Fast DC Electric Arc Detection. *Energies* **2021**, *14*, 288. [[CrossRef](#)]
17. Chen, S.; Li, X.; Xiong, J. Series Arc Fault Identification for Time-Domain and Time-Frequency-Domain Analysis. *IEEE J. Photovolt.* **2017**, *7*, 1105–1114. [[CrossRef](#)]
18. Liu, Y.-J.; Chen, C.-I.; Fu, W.-C.; Lee, Y.-D.; Cheng, C.-C.; Chen, Y.-F. A Hybrid Approach for Low-Voltage AC Series Arc Fault Detection. *Energies* **2023**, *16*, 1256. [[CrossRef](#)]
19. Peng, H.; Zhang, H.; Fan, Y.; Shangguan, L.; Yang, Y. A review of research on wind turbine bearings' failure analysis and fault diagnosis. *Lubricants* **2022**, *11*, 14. [[CrossRef](#)]
20. Yan, J.; Li, Q.; Duan, S. A Simplified Current Feature Extraction and Deployment Method for DC series Arc Fault Detection. *IEEE Trans. Ind. Electron.* **2023**, *71*, 625–634. [[CrossRef](#)]

21. Wang, L.; Lodhi, E.; Yang, P.; Qiu, H.; Rehman, W.U.; Lodhi, Z.; Tamir, T.S.; Khan, M.A. Adaptive Local Mean Decomposition and Multiscale-Fuzzy Entropy-Based Algorithms for the Detection of DC Series Arc Faults in PV Systems. *Energies* **2022**, *15*, 3608. [[CrossRef](#)]
22. Ahn, J.-B.; Jo, H.-B.; Ryoo, H.-J. Real-Time DC Series Arc Fault Detection Based on Noise Pattern Analysis in Photovoltaic System. *IEEE Trans. Ind. Electron.* **2023**, *70*, 10680–10689. [[CrossRef](#)]
23. Yin, Z.; Wang, L.; Zhang, B.; Meng, L.; Zhang, Y. An Integrated DC Series Arc Fault Detection Method for Different Operating Conditions. *IEEE Trans. Ind. Electron.* **2021**, *68*, 12720–12729. [[CrossRef](#)]
24. Bao, J.; Zhang, Y.; Duan, Z.; Zhang, H. Arc fault identification method based on fractal theory and SVM. In Proceedings of the 2014 International Conference on Power System Technology, Chengdu, China, 20–22 October 2014.
25. Seeley, D.; Sumner, M.; Thomas, D.W.P.; Greedy, S. DC Series Arc Fault Detection Using Fractal Theory. In Proceedings of the 2023 IEEE International Conference on Electrical Systems for Aircraft, Railway, Ship Propulsion and Road Vehicles & International Transportation Electrification Conference (ESARS-ITEC), Venice, Italy, 29–31 March 2023.
26. Fontana, C. Fractal Dimension Logarithmic Differences Method for Low Voltage Series Arc Fault Detection. In Proceedings of the 2021 5th International Conference on Smart Grid and Smart Cities (ICSGSC), Tokyo, Japan, 18–20 June 2021.
27. Gao, Y.; Dong, J.; Sun, Y.; Lin, Y.; Zhang, R. PV arc-fault Feature Extraction and Detection Based on Bayesian Support Vector Machines. *Int. J. Smart Grid Clean Energy* **2015**, *4*, 283–290. [[CrossRef](#)]
28. Le, V.; Yao, X.; Miller, C.; Tsao, B. Series DC Arc Fault Detection Based on Ensemble Machine Learning. *IEEE Trans. Power Electron.* **2020**, *35*, 7826–7839. [[CrossRef](#)]
29. Yi, Z.; Etemadi, A.H. Line-to-line Fault Detection for Photovoltaic Arrays Based on Multiresolution Signal Decomposition and two-stage Support Vector machine. *IEEE Trans. Ind. Electron.* **2017**, *64*, 8546–8556. [[CrossRef](#)]
30. Resat, C.; Musa, Y.; Ahmet, G. A voltage scanning-based MPPT method for PV power systems under complex partial shading conditions. *Renew. Energy* **2022**, *184*, 361–373.
31. Ahmet, G.; Hakan, K.; Resat, C.; Musa, Y. Speed Sensorless Adaptive Power Control for Photovoltaic-Fed Water Pump Using Extended Kalman-Bucy Filter. *Energy Rep.* **2023**, *10*, 1785–1795.
32. Zhu, H.; Zhang, D. Influence of multijunction Ga/As solar array in usage in S3R and solving methods for high-power applications. *IEEE Trans. Power Electron.* **2014**, *29*, 179–190. [[CrossRef](#)]
33. Zhu, H.; Zhang, D. Design Considerations of Sequential Switching Shunt Regulator for High-Power Applications. *IEEE Trans. Ind. Electron.* **2020**, *67*, 9358–9369. [[CrossRef](#)]

Disclaimer/Publisher’s Note: The statements, opinions and data contained in all publications are solely those of the individual author(s) and contributor(s) and not of MDPI and/or the editor(s). MDPI and/or the editor(s) disclaim responsibility for any injury to people or property resulting from any ideas, methods, instructions or products referred to in the content.